Available online at www.sciencedirect.com

ScienceDirect

Ceramics International 40 (2014) 3461–3468

CERAMICS INTERNATIONAL

www.elsevier.com/locate/ceramint

Influence of Sb doping on the structural, optical, electrical and acetone sensing properties of In_2O_3 thin films

N.G. Pramod*, S.N. Pandey

Department of Physics, Motilal Nehru National Institute of Technology, Allahabad 211004, India

Received 29 July 2013; received in revised form 11 September 2013; accepted 20 September 2013
Available online 25 September 2013

Abstract

Indium oxide thin films (undoped and Sb doped) have been grown by a chemical spray pyrolysis technique on glass substrates using indium nitrate and antimony trichloride as the host and dopant precursors respectively and deionsied water as the solvent. In addition to studying the acetone sensing properties, the effect of Sb doping on the structural, optical, and electrical properties of In_2O_3 thin film has been investigated. X-ray diffraction analyses reveal that the films are polycrystalline in nature, possess cubic structure, and have crystallite sizes in the range 8–15 nm. The Sb-doped films have reduced crystallinity and crystallite size as compared to the undoped In_2O_3 film. A change in the optical transmittance in the visible region as well as the value of optical band gap is observed upon Sb doping. Further, the incorporation of Sb to In_2O_3 also alters the value of electrical resistivity over a wide range of temperature. The gas sensing properties of the films have been investigated for various concentrations of acetone in air at different operating temperatures. Among all the four films examined, the 1.5 at.% Sb-doped In_2O_3 thin film shows the highest optical transmittance in the visible region, the least electrical resistivity at room temperature and the highest response (~95%) for acetone vapor at an operating temperature of 300 °C and a concentration of 80 ppm in air.

Keywords: In_2O_3 thin film; Spray pyrolysis; Sb-doping; Acetone sensor

1. Introduction

Gas sensors based on semiconducting oxide thin films have drawn considerable attention in recent years because of their widespread use in various industrial and technological applications [1–5]. Transparent Conducting Oxides (TCOs) are suitable candidates for the detection of many Volatile Organic Compounds (VOCs) such as methanol, ethanol, acetone, formaldehyde, etc. [6–10]. Thin films of materials are better in comparison to their bulk counterpart as gas sensing is a surface phenomenon. In this regard, indium oxide (In_2O_3) thin film is a potential material which is being used in a variety of devices because of its good surface conductance to gas adsorption, physical stability, chemical inertness and ease in interfacing with electronic circuits [11–13]. In_2O_3 is an n-type semiconductor possessing both optical direct and indirect band gaps of values about 3.6 eV and 2.8 eV respectively. It also possesses very good electrical conductivity and optical transmittance in the visible region simultaneously [14,15]. In addition to having a large band gap, indium oxide can sustain a high value of mobility and electron concentration. The optical and electrical properties of this oxide material can be engineered by appropriate doping while maintaining desirable stoichiometry [16–18]. It may be noted that the properties of thin films of TCO materials are strongly dependent on the preparation method and control of the process parameters. In this direction, spray pyrolysis has proven to be one of the most crucial and inexpensive techniques for the growth of many TCO materials, including In_2O_3 thin films on glass substrates. This method does not require the use of a vacuum system, and allows large-area coatings and flexibility for doping many elements [19].

Acetone, a VOC, is a laboratory solvent for many plastics and some synthetic fibers. It is a common solvent for rinsing laboratory glassware because of its low cost and volatility. Inhalation of high concentrations of acetone vapor in the air causes irritation of the throat and eyes in a few minutes [20,21].

*Corresponding author. Tel.: +91 73883 44147; fax: +91 532 2445077.
E-mail address: pramodng@gmail.com (N.G. Pramod).

0272-8842/$ - see front matter © 2013 Elsevier Ltd and Techna Group S.r.l. All rights reserved.
http://dx.doi.org/10.1016/j.ceramint.2013.09.084

Due to all of the above, there is an urgent need for an acetone sensor that has the capability to detect very low amounts of the vapor and that can afford good recovery.

Although a variety of metal ions, including transition and alkali metal ions (Mo, W, Eu, Mg, etc.), have been doped to In_2O_3 thin film and the resulting properties have been studied [22–25], very few reports are available on the doping of antimony on In_2O_3 [26,27]. This motivates us to choose antimony as the dopant ion for our present work. A detailed investigation as to how the structural, optical, electrical and acetone sensing properties of In_2O_3 thin film are altered by Sb doping is the objective of the present study. It is worth mentioning that the acetone sensing properties of sprayed Sb-doped In_2O_3 thin film are reported for the first time here, to the best of authors' knowledge.

2. Experimental

Undoped In_2O_3 and Sb:In_2O_3 thin films have been grown by a chemical spray pyrolysis technique on clean glass substrates. The precursors used for the synthesis of the films were indium nitrate $In(NO_3)_3$ (Sigma Aldrich) and antimony (III) chloride $SbCl_3$ (Merck) and deionised water as the solvent. The substrates were cleaned prior to deposition, first by rinsing with freshly prepared chromic acid and deionized water, and then ultrasonically with trichloroethylene for about 30 min. Then they were washed with deionized water again and finally dried in air. A schematic representation of the spray apparatus has been shown in Fig. 1. The precursor solution was sprayed through a locally designed glass nozzle on the hot substrates with pressurized air being the carrier gas. The various process parameters for the film deposition are listed in Table 1. The thicknesses of the resulting films prepared by spraying 3 ml of the respective solutions were estimated by the weight-difference method using an electronic precision balance (Citizen, Model: CX 165) and were found to be in the range 200–250 nm. The films thus prepared were subjected to structural, optical, electrical and acetone sensing studies.

The films were examined by X-ray diffraction (XRD) for structural characterization and analysis. The same was carried out using a PANalytical X'Pert PRO with CuKα radiation

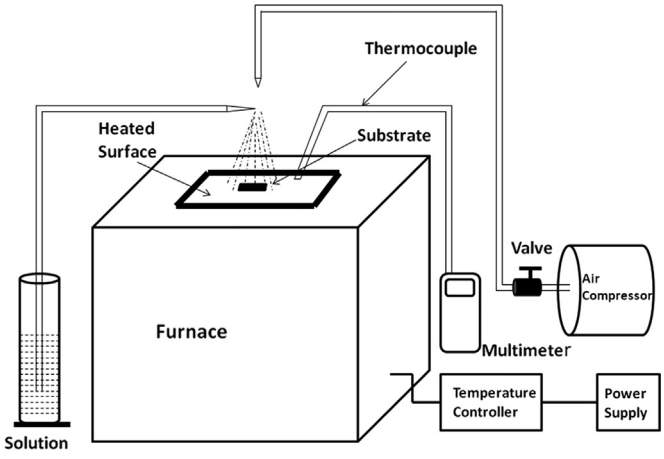

Fig. 1. Schematic setup of spray pyrolysis equipment.

Table 1
Process parameters for the spray deposition of the films.

Spray parameters	Optimum value/item
Substrate temperature	400 ± 10 °C
Precursors used	Indium nitrate $In(NO_3)_3$ & antimony trichloride $SbCl_3$
Solvent	Deionised water
Substrate	Glass
Substrate–nozzle distance	15 cm
Carrier gas pressure	3 kg/cm^2
Solution flow rate	3 ml/min
Solution concentration	0.1 M

($\lambda = 1.5406$ Å) as the X-ray source at 30 mA, 30 kV, the scanning angle 2θ varying from 20° to 65° at a scan speed of 0.02° per second. The films were then examined for surface roughness and morphology by an NTEGRA atomic force microscope (AFM). In order to determine the band structure and energy band gap, a Perkin Elmer Lambda 35 UV–vis spectrophotometer (UK) was used and the samples were scanned in the wavelength range 300–800 nm and their corresponding values of transmittance and absorbance were recorded. Highly conducting silver was applied on both ends of the films for making ohmic contacts. The film was mounted on a two-probe assembly placed into a silica tube, which was inserted coaxially inside a resistance-heated furnace. The experimental setup employed to study the sensing characteristics of the films was a static system, described elsewhere [14]. The electrical resistance of the films was measured before and after exposure to acetone vapor using a Keithley System Electrometer model 6517B. The measurement of acetone concentration was carried out by taking required amount of liquid acetone in a Hamilton micro-syringe and then injecting it into the glass tube. The sensor response of the film was determined at different operating temperatures, in the range 200–300 °C for various concentrations of acetone in air.

3. Results and discussion

3.1. Structural and morphological analysis

Fig. 2 presents the XRD patterns of the undoped and Sb-doped In_2O_3 thin films. The patterns have been indexed with JCPDS card no. (06-0416) and it was found that the films are polycrystalline In_2O_3, with the crystal structure being cubic. No phases corresponding to antimony or any other antimony compound have been detected in the XRD patterns. The crystallite size has been evaluated from the well known Scherrer formula and the average values of the crystallite size have been listed in Table 2. The texture coefficient has been calculated to describe the preferential orientation ($h\,k\,l$) using the following expression:

$$TC(h\,k\,l) = \frac{I(h\,k\,l)/I_0(h\,k\,l)}{(1/N)\sum_N I(h\,k\,l)/I_0(h\,k\,l)} \quad (1)$$

where N is the number of diffraction peaks, $I(h\,k\,l)$ and $I_0(h\,k\,l)$ are the measured and corresponding recorded intensities of the

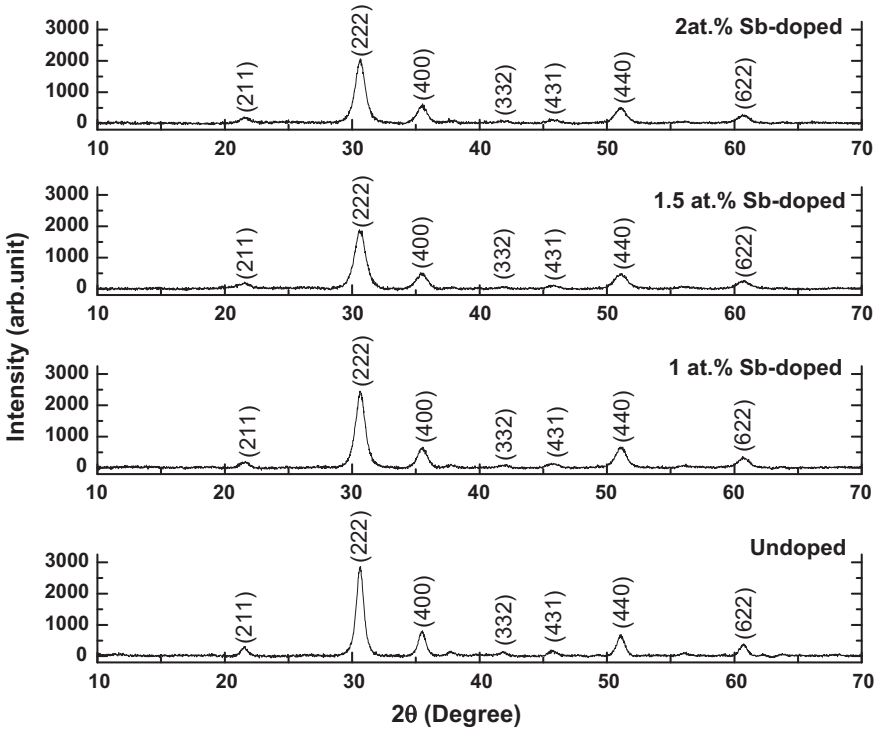

Fig. 2. XRD patterns of the undoped and Sb-doped In_2O_3 thin films.

Table 2
Structural parameters of the undoped and Sb-doped thin films.

In_2O_3 films	XRD analyses					AFM average surface roughness (nm)
	Average crystallite size (nm)	Lattice parameter $a=b=c$ [Å]	Average lattice strain	Texture coefficient (TC)		
				(2 2 2) plane	(4 0 0) plane	
Undoped (0 at.% Sb)	14.1	10.11	0.008	1.36	1.22	11.2
1 at.% Sb	9.8	10.11	0.012	1.46	1.27	8.6
1.5 at.% Sb	8.3	10.12	0.014	1.34	1.20	4.4
2 at.% Sb	9.8	10.12	0.012	1.37	1.28	2.6

diffraction peaks according to JCPDS (06-0416) card respectively. The value of the texture coefficient indicates that the maximum preferred orientation of the films is along the diffraction plane. This means that the increase in preferred orientation is associated with increase in the number of grains along that plane. In the present case, changes in the value of texture coefficient are seen because of Sb doping in the In_2O_3 film, which have been presented in Table 2. It is observed that both the crystallite size and the intensities of the two strongest peaks (2 2 2) and (4 0 0) tend to reduce upon Sb doping. The reduction in crystallite size is attributed to the enhancement in the density of nucleation centers in the doped films. Since the ionic radius of the Sb^{3+} ion (0.76 Å) is smaller than that of the In^{3+} ion (0.8 Å), there is a creation of compressive stress in the films on Sb doping. This may be the reason for the reduction in both of the above observed parameters. Further, poor crystallinity in the Sb-doped films is due to the fact that the Sb incorporation in the In_2O_3 film matrix enables more nucleation sites, thereby inhibiting the growth of crystal grains.

The undoped and the Sb-doped thin films were analyzed by atomic force microscopy for surface morphology studies and the respective 2D and 3D AFM images have been presented in Figs. 3 and 4, respectively. The samples were scanned in an area of 1 μm × 1 μm. All the films show non-spherical, island growth consisting of continuous grains. It is clear that the incorporation of antimony affects the morphology of the indium oxide film surface. The values of the various parameters evaluated from AFM analyses, viz., the grain size and surface roughness, have a marked difference on Sb doping. In fact, as evident from Table 2, the doping of Sb metal ion reduces the grain size and the surface roughness of the undoped film.

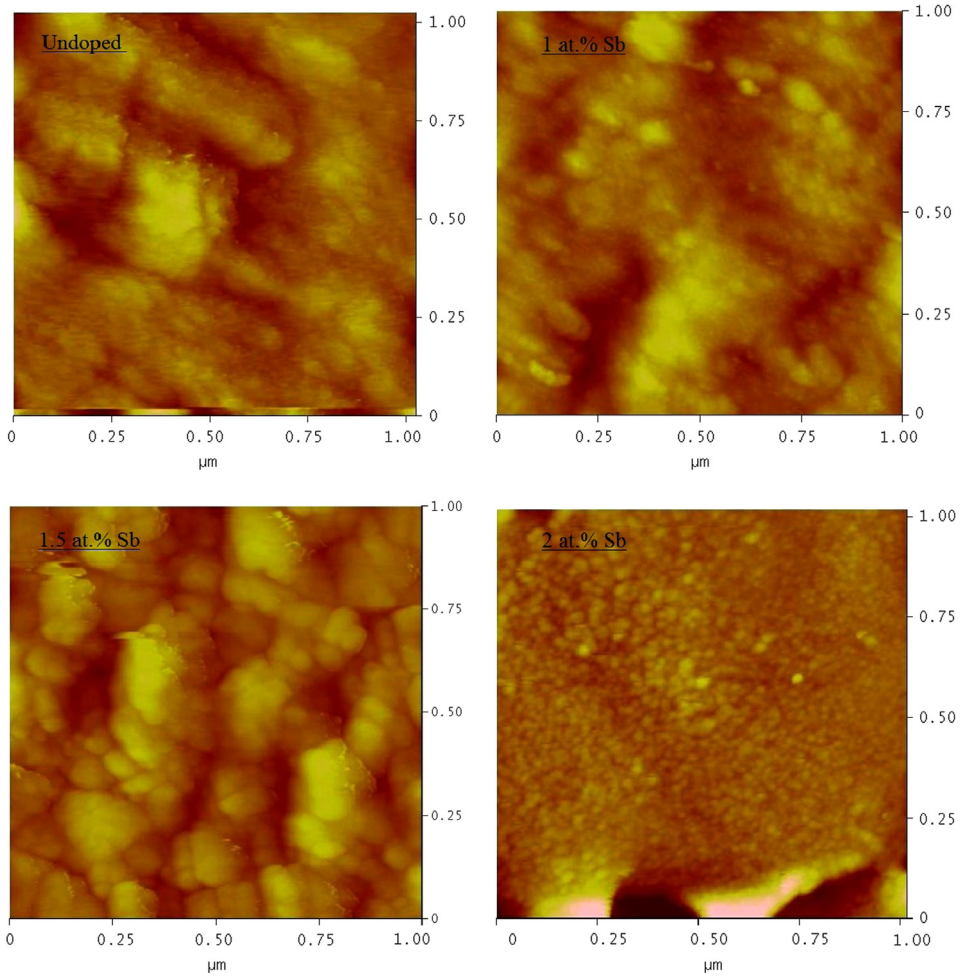

Fig. 3. 2D AFM images of undoped and Sb-doped films.

3.2. Optical studies

Analysis of optical data is an important tool for understanding the band structure and energy band gap of crystalline TCOs. Keeping this in view, the undoped and the Sb-doped films have been subjected to optical characterization. Figs. 5 and 6 illustrate the transmittance and absorbance spectra, of the undoped and Sb-doped In_2O_3 thin films in the wavelength range 300–750 nm respectively. As evident from Fig. 5, doping of Sb ions influences the optical transmittance of In_2O_3 thin films. The value of transmittance of the 1.5 at.% Sb sample is greater as compared to all other samples in the entire range of the wavelengths where the data is taken. Since the values of the crystallite size and the average grain size (evaluated from XRD and AFM analyses respectively, Table 2) for the 1.5 at.% Sb sample are the lowest, the energy loss due to light scattering and a reduction of lattice defects are low in comparison with other films, thus rendering good optical transmittance. This lower energy loss promotes the optical transmittance to a good extent and this sample records a value of 99% transmittance at a wavelength of 700 nm. Further, the values of the optical transmittance in the 1 and 2 at.% Sb samples are low as compared to that of the undoped and the 1.5 at.% Sb films. Enhanced scattering loss due to discontinuous grain growth and strain effects arising due to lattice mismatch between the crystalline film and the amorphous substrate at the time of deposition could be factors for the low values of transmittance in these films.

The variation of $(Ah\nu)^2$ and the photon energy $h\nu$ is shown in Fig. 7. The value of the band gap is estimated by extrapolating the linear portion of $(Ah\nu)^2 \rightarrow 0$. It is inferred from the figure that the value of the direct band gap changes on Sb doping. Fig. 8 illustrates the dependence of the optical direct band gap with the AFM grain size as a function of the Sb dopant concentration. The variation of the value of the direct optical band gap in the present study is found to be consistent with the values of the grain size evaluated from AFM analyses for all the samples. The enhancement in the band gap values in the 1 at.% Sb and 2 at.% Sb doped films as compared to the undoped film could be due to quantum confinement effects [28]. In nanostructured materials, an increase of the band gap energy is seen because of localization of charges in individual nanocrystals. As compared to their bulk counterpart, the shift in the values of the band gap in nanocrystalline thin films towards higher $h\nu$ values can be due to quantum confinement effects because of

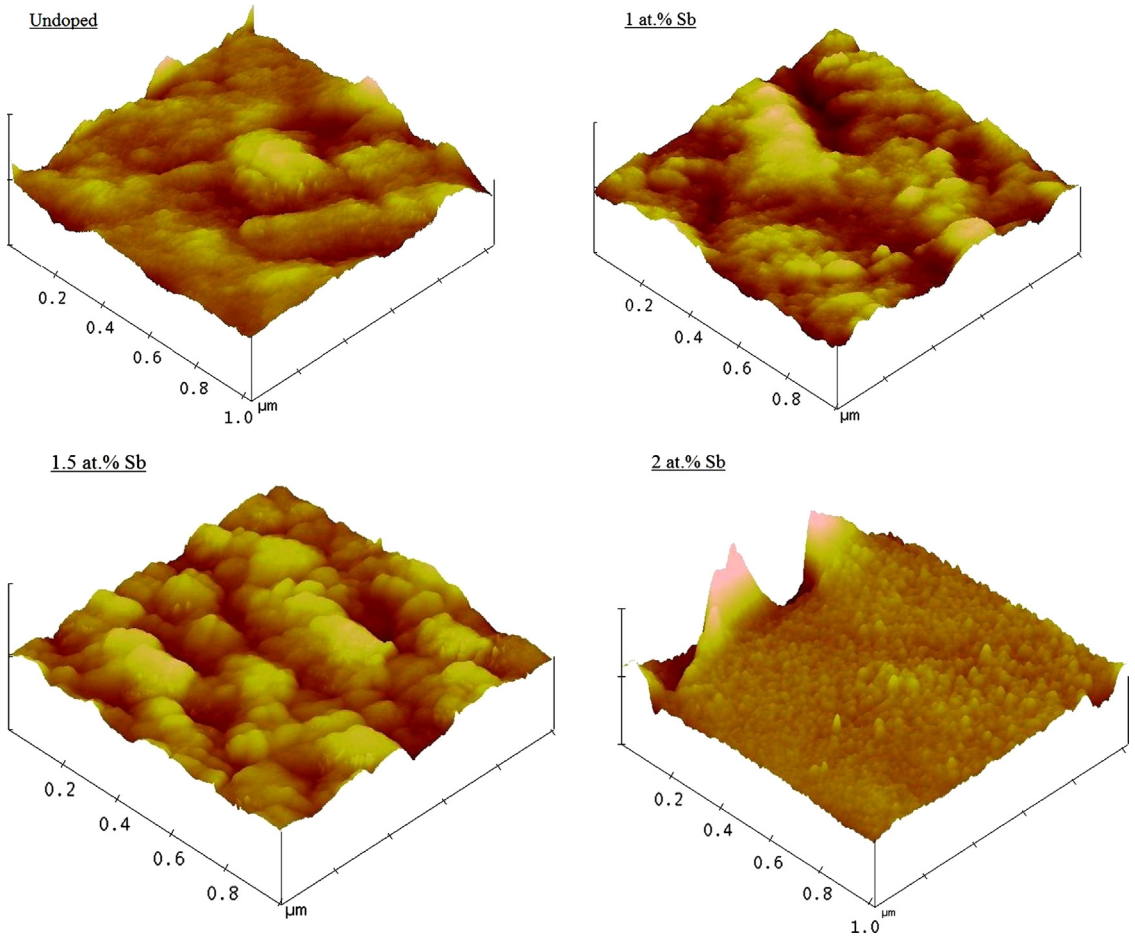

Fig. 4. 3D AFM images of undoped and Sb-doped films.

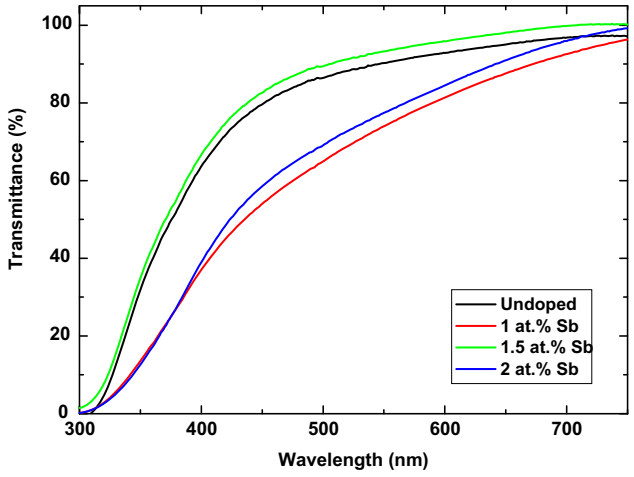

Fig. 5. Transmittance spectra of the undoped and the Sb-doped films.

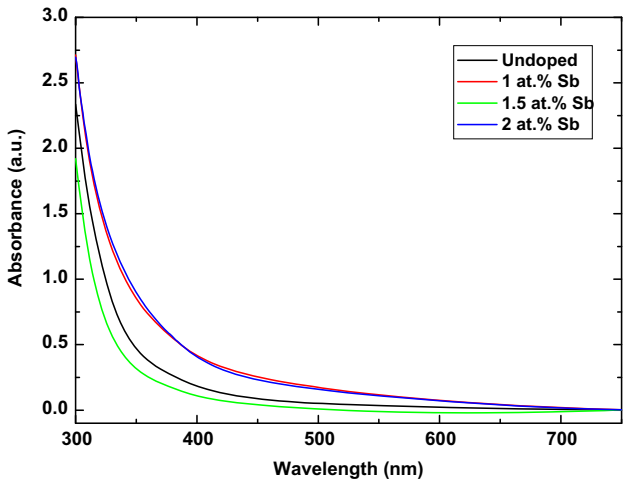

Fig. 6. Absorbance spectra of the undoped and the Sb-doped films.

the formation of quantum dots of very small dimension [28]. Further, for the 1.5 at.% Sb doped film, a reduction of defects at the grain boundaries of the layers in the microstructure leads to the observed increase in the band gap. An enhancement in the electron concentration leads to a rise in the Fermi level within the conduction band, causing the increase in the value of the band gap for this sample [29].

3.3. Electrical studies

The variation of electrical resistivity of the undoped and the Sb-doped films in the temperature range 25–300 °C is shown in Fig. 9. It has been observed, from the figure, that the incorporation of Sb ions has an influence over the In_2O_3 films as the value of electrical resistivity changes in the whole

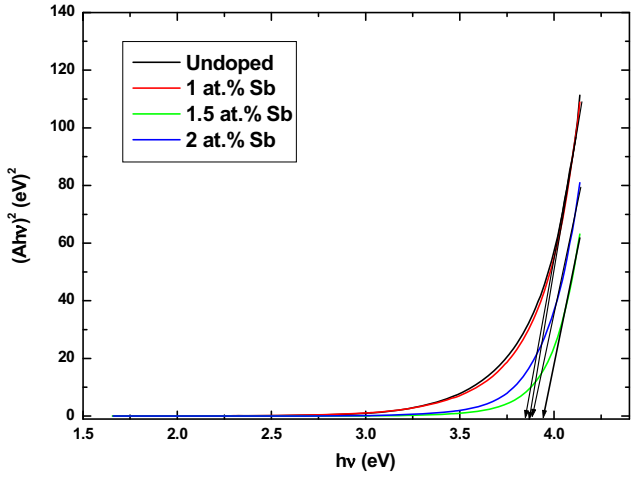

Fig. 7. Variation of direct optical band gap with photon energy $h\nu$.

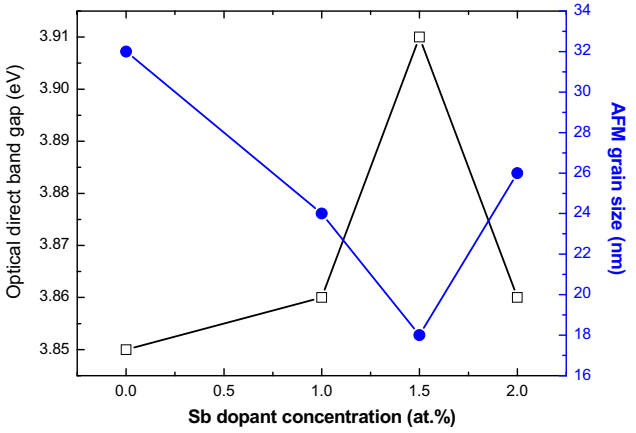

Fig. 8. Dependence of optical band gap with grain size as a function of Sb dopant concentration.

temperature range of 25–300 °C. The electrical resistivity of the Sb-doped films decreases as compared to the undoped film in the range 25–175 °C and thereafter, it begins to increase. In fact, the 1.5 at.% Sb-doped In_2O_3 sample film shows the lowest electrical resistivity even at room temperature, the temperature at which most of the devices operate.

For the undoped film, it is observed that the resistance of the film first increases with temperature up to 75 °C, which is because of adsorption of atmospheric oxygen on the film surface. In the temperature range 125–200 °C, the film resistance decreases rapidly with rise in temperature, while decrease in resistance is slower in the temperature range 200–300 °C. In fact, two competing processes of thermal excitation of electrons and oxygen adsorption occur simultaneously [14]. The sharp reduction in film resistance in the temperature range 125–200 °C is because the thermal excitation of electrons dominates over the oxygen adsorption process, while the gradual decrease in the film resistance with temperature in the range 200–300 °C may be the result of improved adsorption of atmospheric oxygen at higher temperatures.

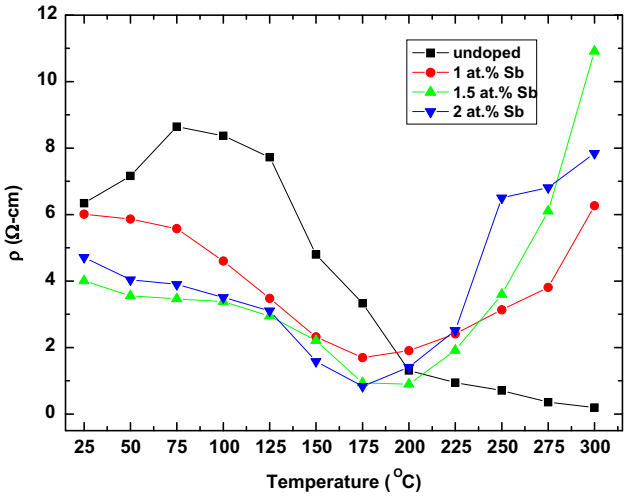

Fig. 9. Dependence of electrical resistivity with temperature for the undoped and Sb-doped films.

For the Sb-doped films, the electrical resistance first decreases up to a temperature of about 175 °C, and thereafter it increases. Sb ion species are considered to be electron donors and they serve to increase the carrier concentration and decrease the electrical resistivity. This phenomenon occurs up to a temperature of 175 °C. However, after a temperature of 200 °C, the mobility of the electrons decreases and the impurities may precipitate, resulting in defect structures which would trap electrons to cause an increase in resistivity. Similar results have also been observed by Lee and Huang [30]. Further, because the films are polycrystalline in nature, the high resistivity could be due to grain boundary effects. Since air is used as the carrier gas for the growth of the films, it is probable that a large number of oxygen molecules are chemisorbed in the film at the grain boundaries and this might lead to an increase in the value of electrical resistivity of the Sb-doped films [11].

3.4. Acetone sensing characteristics

The sensing mechanism of acetone vapor to In_2O_3 is a surface phenomenon. The sensing response (S) of the film has been defined as the ratio of change in film resistance upon exposure to gas (acetone) to the film resistance in air (at the same operating temperature) and is given by the equation

$$S = \frac{R_a - R_g}{R_a} \times 100\% \quad (2)$$

where R_a is the resistance in air and R_g is the resistance upon exposure to vapor (acetone).

Fig. 10 presents the response characteristics of the films as a function of the operating temperatures (200–300 °C) at four different acetone vapor concentrations viz. 20, 40, 60 and 80 ppm in air. From the response characteristics, it is clear that the 1.5 at.% Sb-doped In_2O_3 thin film shows the highest response for acetone vapor in comparison with other films under study. A response of 95% is recorded for this sample at a concentration of 80 ppm and an operating temperature of 300 °C. Even at an operating temperature of 200 °C and at a concentration of

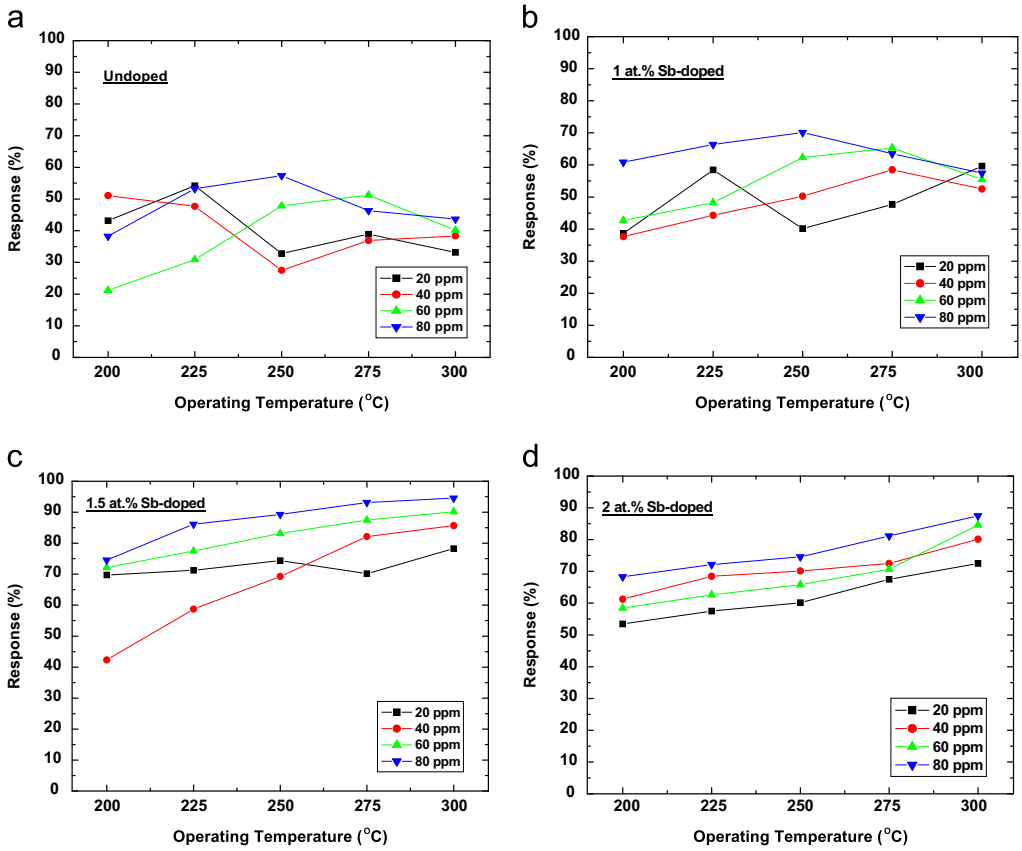

Fig. 10. Response characteristics of (a) undoped, (b) 1 at.%, (c) 1.5 at.% and (d) 2 at.% Sb-doped In_2O_3 thin films as a function of operating temperature.

80 ppm, it shows a response of 75%. This sample has the smallest grain size, which leads to an increase in the surface area of the film exposed to atmosphere, resulting in more adsorption of oxygen species on the film surface and thus creating a number of sensing sites. The dopant ion creates some vacant sites into the host In^{3+} lattice which causes more oxygen from the atmosphere to attach and interact with the conduction electrons, thus converting into active sites. Surface roughness as well as the presence of voids in the film also contributes to the enhancement in the sensor response since they result in larger contact area with the gaseous species. The rapid increase in response is attributed to the availability of sufficient adsorbed oxygen species on the film surface as well as the enhanced chemical activation of acetone molecules.

Atmospheric oxygen is adsorbed on the film surface, when In_2O_3 thin films are heated in air at a temperature greater than 200 °C. In fact, at lower temperatures, the surface reactions proceed too slowly to be useful, while at higher temperatures the increased promotion of electrons into the conduction band tends to obscure the effects of the gases to be detected. The adsorbed oxygen forms ionic species such as O^{2-}, O_2^-, and O^- which acquire electrons from the conduction band and desorb from the surface. So in the temperature range used in the present investigation, only O^- species react with the acetone molecules. The reaction kinetics is given as follows [21]:

$$CH_3COCH_3\ (gas)+O^- \rightarrow CH_3CO^+H_2+OH^-+e^- \quad (3)$$

$$CH_3COCH_3\ (gas)+OH^- \rightarrow CH_3CHO+CH_3O^- \quad (4)$$

$$CH_3CHO+O(bulk) \rightarrow CH_3CHOH+O(vacancies) \quad (5)$$

$$CH_3COCH_3\ (gas)+O^- \rightarrow CH_3C^+O+CH_3O^- \quad (6)$$

$$CH_3C^+O \rightarrow C^+H_3+CO \quad (7)$$

$$CO+O^- \rightarrow CO_2+e^- \quad (8)$$

Thus, once the film is exposed to acetone vapor, the formation of carbon dioxide by the oxidation of acetone leads to the liberation of electrons into the conduction band, resulting in a decrease in the film resistance. The comparative responses of the undoped and the (1, 1.5 and 2 at.%) Sb-doped films as a function of the acetone vapor concentration at an operating temperature of 300 °C have been presented in Fig. 11. It is evident that the incorporation of Sb ions increases the sensor response in all doped films for all concentrations. Further, the 1.5 at.% Sb-doped sample shows the highest response as compared to all other films at the operating temperature of 300 °C for all concentrations of acetone vapor in air. Fig. 12 presents the response and recovery times of the 1.5 at.% Sb-doped film toward acetone vapor with increasing concentrations at 300 °C for which the film shows maximum response. The film shows fast response and recovery to acetone vapor.

4. Conclusion

Indium oxide thin films with crystallite size in the range 8–15 nm were grown by a conventional spray pyrolysis equipment. It is demonstrated that the introduction of Sb has

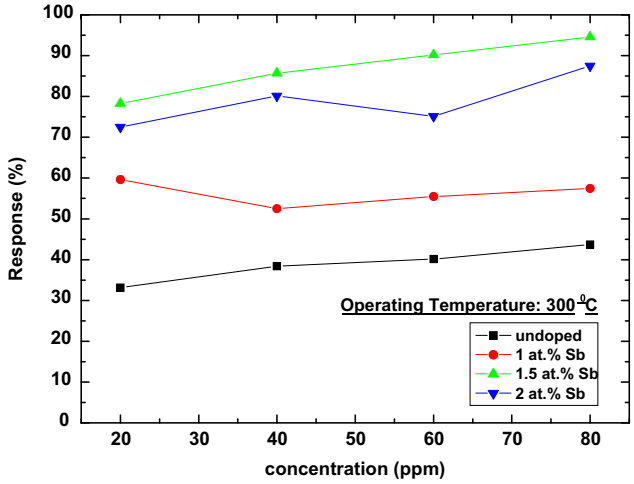

Fig. 11. Comparative responses of the undoped and the Sb-doped films as a function of the acetone vapor concentration at an operating temperature of 300 °C.

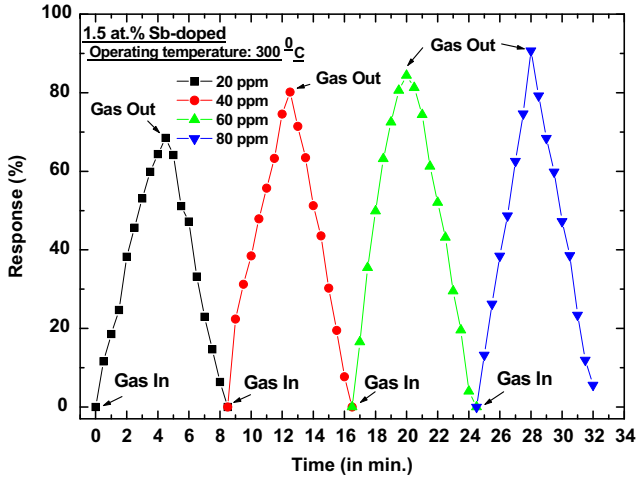

Fig. 12. Response and recovery times of the 1.5 at.% Sb-doped film towards acetone vapor with increasing concentrations at the operating temperature of 300 °C.

a good influence on the microstructural, optical and electrical properties along with enhancing the response of the In_2O_3 film for acetone vapor. The deposited films confirm the cubic phase of indium oxide. The transmittance in the visible region differs between the undoped and the Sb-doped samples. The 1.5 at.% Sb-doped film exhibits the highest optical transmittance (~99%) and the lowest value of electrical resistivity at room temperature, in addition to the enhanced sensor response of 95% for acetone vapor at an operating temperature of 300 °C for a concentration of 80 ppm in air. According to our results, we conclude that the 1.5 at.% Sb:In_2O_3 film is a promising material for various optoelectronic applications and as a sensor element in acetone sensing devices.

Acknowledgments

The authors are thankful to Mr. Ajay Kushwaha, Department of Physics, Indian Institute of Technology, Bombay, India, for providing XRD and AFM facilities. Further, the authors are grateful to Professor P.P. Sahay for useful discussions.

References

[1] G. Neri, A. Bonavita, G. Rizzo, S. Galvagno, S. Capone, P. Siciliano, Sensors and Actuators B 114 (2006) 687–695.
[2] A. Teeramongkonrasmee, M. Sriyudthsak, Sensors and Actuators B 66 (2000) 256–259.
[3] Preeti Pandey, J.K. Srivastava, V.N. Mishra, R. Dwivedi, Journal of Natural Gas Chemistry 20 (2011) 123–127.
[4] Zheng Jiao, Minghong Wu, Jianzhong Gu, Xilian Sun, Sensors and Actuators B 94 (2003) 216–221.
[5] A. Galdikas, Z. Martūnas, A. Šetkus, Sensors and Actuators B 7 (1992) 633–636.
[6] Bong-Chull Kim, Jae-Yeol Kim, Duk-Dong Lee, Jeong-Ok Lim, Jeung-Soo Huh, Sensors and Actuators B 89 (2003) 180–186.
[7] N.G. Patel, P.D. Patel, V.S. Vaishnav, Sensors and Actuators B 96 (2003) 180–189.
[8] V.S. Vaishnav, P.D. Patel, N.G. Patel, Thin Solid Films 490 (2005) 94–100.
[9] P.P. Sahay, R.K. Nath, Sensors and Actuators B 134 (2008) 654–659.
[10] L.A. Patil, M.D. Shinde, A.R. Bari, V.V. Deo, Current Applied Physics 10 (2010) 1249–1254.
[11] P.K. Manoj, K.G. Gopchandran, Peter Koshy, V.K. Vaidyan, Benny Joseph, Optical Materials 28 (2006) 1405–1411.
[12] A. Moses, Ezhil Raj, K.C. Lalithambika, V.S. Vidhya, G. Rajagopal, A. Thayumanavan, M. Jayachandran, C. Sanjeeviraja, Physica B 403 (2008) 544–554.
[13] V.S. Vaishnav, P.D. Patel, N.G. Patel, Thin Solid Films 487 (2005) 277–282.
[14] N.G. Pramod, S.N. Pandey, P.P. Sahay, Ceramics International 38 (2012) 4151–4158.
[15] N.G. Pramod, S.N. Pandey, P.P. Sahay, Journal of Thermal Spray Technology 22 (2013) 1035–1043.
[16] D. Beena, K.J. Lethy, R. Vinodkumar, A.P. Detty, V.P. Mahadevan Pillai, V. Ganesan, Journal of Alloys and Compounds 489 (2010) 215–223.
[17] P. Prathap, G. Gowri Devi, Y.P.V. Subbaiah, K.T. Ramakrishna Reddy, V. Ganesan, Current Applied Physics 8 (2008) 120–127.
[18] C. Coutal, A. Azema, J.-C. Roustan, Thin Solid Films 288 (1996) 248–253.
[19] M. Ait Aouaj, R. Diaz, A. Belayachi, F. Rueda, M. Abd-Lefdil, Materials Research Bulletin 44 (2009) 1458–1461.
[20] Salim F. Bamsaoud, S.B. Rane, R.N. Karekar, R.C. Aiyer, Sensors and Actuators B 153 (2011) 382–391.
[21] Qi Qi, Tong Zhang, Li Liu, Xuejun Zheng, Qingjiang Yu, Yi Zeng, Haibin Yang, Sensors and Actuators B 134 (2008) 166–170.
[22] A. Moses, Ezhil Raj, V. Senthilkumar, V. Swaminathan, Joachim Wollschläger, M. Suendorf, M. Neumann, M. Jayachandran, C. Sanjeeviraja, Thin Solid Films 517 (2008) 510–516.
[23] S. Parthiban, V. Gokulakrishnan, K. Ramamurthi, E. Elangovan, R. Martins, E. Fortunato, R. Ganesan, Solar Energy Materials and Solar Cells 93 (2009) 92–97.
[24] Q. Zhang, X. Li, G. Li, Thin Solid Films 517 (2008) 613–616.
[25] E. Elangovan, G. Gonçalves, R. Martins, E. Fortunato, Solar Energy 83 (2009) 726–731.
[26] J. Choisnet, L. Bizo, R. Retoux, B. Raveau, Solid State Sciences 6 (2004) 1121–1123.
[27] M.V. Vinokurova, L.E. Derlyukova, A.A. Vinokurov, Inorganic Materials 43 (2007) 1085–1092.
[28] D. Beena, K.J. Lethy, R. Vinodkumar, V.P. Mahadevan Pillai, V. Ganesan, D.M. Phase, S.K. Sudheer, Applied Surface Science 255 (2009) 8334–8342.
[29] P. Prathap, Y.P.V. Subbaiah, M. Devika, K.T. Ramakrishna Reddy, Materials Chemistry and Physics 100 (2006) 375–379.
[30] C.H. Lee, C.S. Huang, Materials Science and Engineering B 22 (1994) 233–240.